Study of the influence of crystalline phases on optical characteristics of a glass-ceramic in the visible range via simulations by the four-flux method

Sandra Rio, Christine Andraud, Philippe Deniard, Catherine Dacquin, Rodolphe Delaval, Sébastien Donze, Stéphane Jobic

Study of the influence of crystalline phases on optical characteristics of a glass-ceramic in the visible range via simulations by the four-flux method

Sandra RIO[a,b], Christine ANDRAUD[c], Philippe DENIARD[b], Catherine DACQUIN[a], Rodolphe DELAVAL[a] , Sébastien DONZE[a] and Stéphane JOBIC[b]

[a] *Arc France, 104 avenue du Général de Gaulle, 62510 Arques, France*
[b] *Université de Nantes, CNRS, Institut des Matériaux Jean Rouxel, IMN, F-44000 Nantes, France*
[c] *Centre de Recherche sur la Conservation des Collections, USR 3224, MNHN, 36 rue Geoffroy Saint-Hilaire, 75005 Paris, France*

Corresponding author. philippe.deniard@cnrs-imn.fr

Key words: glass-ceramics, opal glass, light scattering, four-flux method, opacity, CIELab parameters

ABSTRACT

Opal glasses fabricated by Arc (Arques, France) are glass-ceramics that consist of a glassy matrix mainly constituted of silicon dioxide with well crystallized fluoride compounds as inclusions. These later (ca. 8 vol%) play the role of light scattering centers leading to the well-known milky feature of the commercialized glassware, dinnerware products. Their overall chromatic characteristics strongly depend on few parameters (e.g. the refractive indexes of the glass and the ceramic(s), the concentration of inclusions, their mean size, the surface roughness of the article, etc) that have to be determined and controlled during the manufacturing process to end at the product with the desired optical properties. Using a transfer matrix formalism, the 4-flux method can indeed be used to anticipate the transmittance and reflectance of an object for different set of parameters. The impact of each aforementioned parameter on the color rendering will be here separately discussed, and simulations will be confronted to experimental data to assert their validity and their interest to the genesis of new products with targeted optical properties.

1. INTRODUCTION

Desired colorless oxide glasses can be unfortunately obtained as colored materials if no attention is paid to the purity of the pristine materials. Formally, these ones often contain metal oxides, as traces or in significant amounts, that can (unintentionally) incorporate the final chemical composition of the product at the fusion step. This may induce a large panel of colors[1]. Hence, in silicate based glasses (e.g. soda lime), the presence of Fe^{2+} cations will trigger the well-known blue-green tint of wine bottles, while Fe^{3+} and Co^{2+} cations will favor pale yellow or deep blue recipients, respectively. Namely, color is then dictated by the nature of the light absorbing transition metal cation, its chemical environment (that controls the splitting of the orbital d-block), its concentration, and its oxidation state. Hue can also originate from lanthanides as Nd^{3+}, Pr^{3+}, Er^{3+}, etc. Formally, it can turn out to be in practice much more intricate to achieve colorless glasses than colored ones, even if when desired, these latter require also stringent elaboration conditions for reproducibility. Color in glasses may also be due to small metallic aggregates[2] (e.g. gold ruby red or silver yellow nanoparticles) that grew up within

the glass with specific size and morphology or to semiconducting inorganic pigments (e.g. red Cu_2O, yellow CdS) encapsulated in the vitreous matrix[3,4]. Absorption properties are governed by surface plasmon resonance phenomena in the former case and by the promotion of electrons from the valence band to the conduction band in the latter case. Color may also be produced by mechanisms other than absorption, namely by light scattering[5]. Hence, opal glasses with a translucent to an opaque milky feature can be manufactured with crystalline phases (commonly fluoride compounds) that germinate and grow within the glass during the cooling process[6]. This is the topic of the present contribution.
Namely opal glasses are glass-ceramics defined by J. Deubener et *al.*[7] as *inorganic, non-metallic materials prepared by controlled crystallization of glasses via different processing methods.* These composites contain one or several crystalline phases entrapped in a glass and vice versa and constitute a new state of matter with often extraordinary mechanical, thermal, electrical and optical properties[8]. The fraction of crystalline phase may range from a few parts per million by volume to almost 100%, and this fraction will be strongly dependent of the elaboration protocol, and the cooling kinetics in particular. Concerning optical properties, the inclusion of uncolored crystals within a colorless glass can lead to a bluish (and even reddish in transmission) tint or a white color. In the former case (Rayleigh regime), the impinging light will interact with very small particles and will be scattered in all directions of the space with an intensity proportional to the inverse fourth power of the wavelength[9]. This intensity will also depend on the particle size and the difference of reflective index between the scattering particle and the medium. Namely, Rayleigh diffusion dictates the blue color of the sky, eyes, feathers of some birds or wings of butterflies, etc. In the latter case (Mie regime), scattering particles are much larger than previously and of the same order of magnitude than the wavelength of the incident light. Then, this one is scattered preferentially in the forwards direction for all wavelengths with a dependence (damped sinusoidal function) with the size parameter, i.e. a parameter proportional to the particle diameter over the incident wavelength ratio[10]. Namely, the white color of clouds, milk and other colloidal solutions originate from a Mie phenomenon with diffusion of light by a few hundred nanometer diameter particles with a refraction index different from the medium[11]. Of course, all intermediate color tint between the Rayleigh blue color and the Mie white color can be observed (in reflection) vs. the particle size, their concentration, the refractive index, etc. This explains why opal glasses can be transparent and colorless, or opaque and white with a possible shiny glint depending on the roughness of under focus shaped material.

Hereafter, the identification of the parameters affecting the visual appearance of an opal glass (plate) manufactured by Arc France is undertaken. Scattering effects of fluoride particles embedded in a SiO_2 based vitreous medium have been simulated by the 4-flux method using a transfer matrix formalism. More specifically, structural and microstructural parameters involved in the color mechanism in this glass-ceramic are separately discussed to determine their direct impact on the final aspect of the object.

2. EXPERIMENTAL SECTION

2.1. Synthesis

Opal glasses are obtained by melting precursors (e.g. SiO_2, Na_2CO_3, $CaCO_3$, Al_2O_3, etc.) in a cold-top furnace at approximately 1500 °C. Then, from a casting around 1100 °C, forming machines give the final shape to the glass articles that are subsequently quenched in air to achieve specific optical and mechanical properties. The resulting glass-ceramics are characterized by a milky white color and exhibit a remarkable shock-absorbing capacity. These

composite materials consist of a glassy matrix (92 wt%) mainly built upon silicon dioxide with crystalline fluoride phases (8 wt%) as inclusions. The opalescent effect is induced by the presence of well crystallized and colorless NaF and CaF_2 compounds. No coloring agents were added to the composition. The glass will be considered as pure SiO_2 hereafter for simulations, the other components being introduced in the melt in much lower amount.

To validate the modeling of colorimetric parameters, a range of samples has been synthesized by varying the fluorine content from the initial composition (**Figure 1**). This induces a modification on the crystallization of NaF and CaF_2 compounds which influences directly the scattering effect. The vitreous matrix compositions are considered to be similar for all the samples leading to no change in the refractive index of the medium from one sample to another.

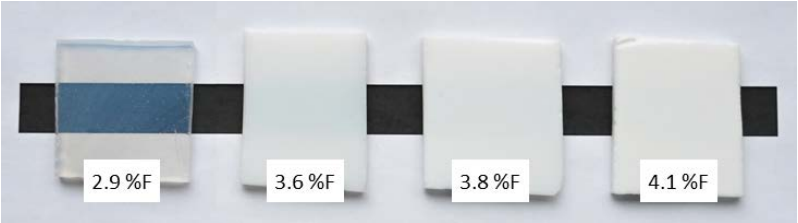

Figure 1: Four samples manufactured by Arc France by varying the fluorine (F atom) concentration from 2.9 to 4.1 wt%.

2.2. XRD, SEM analyses, and optical measurements

All samples were first ground before characterization by X-Ray Diffraction (XRD) techniques to determine the crystallite size of NaF and CaF_2 and their volume fraction. The mass fraction of the vitreous matrix has been determined by adding a 7 wt% of crystallized MgO as a standard to the powdered sample. The refinement results obtained from a Rietveld analysis are summed up in Table 1.

Table 1: Evolution of the size (mean diameter) and the volume fraction of NaF and CaF_2 particles vs. the weight fluorine concentration (data issued from a Rietveld refinement of XRD powder patterns).

%wt of Fluorine (F atom)	NaF cristallite size (nm)	%volume of NaF cristallites	CaF_2 cristallite size (nm)	%volume of CaF_2 cristallites
2.9	27.2 (9)	1.8 (5)	-	-
3.6	96 (5)	5.8 (8)	25.8 (9)	0.6 (3)
3.8	120 (5)	5.8 (5)	36.0 (8)	1.5 (2)
4.1	190 (13)	6.4 (5)	36.6 (9)	1.6 (2)

Once the size of crystallites determined, SEM images were collected on a JEOL JSM 7600F (with a voltage of 7 kV and a 15 mA current). They clearly evidence that particles and crystallites are virtually one, that is particles and crystallites have the same size and grains are limited to one particle only. This peculiar feature is of importance since grain size which is the relevant parameter for scattering properties can be directly obtained from XRD. As crystallites (particles) are well separated from each other, they can indeed be regarded as isolated nanoparticles. Then, transmission and reflection spectra were collected in the visible range (380-780 nm) on 3.5 mm thick (1 by 1 cm^2) plates with a PerkinElmer Lambda 1050 spectrophotometer.

3. THEORETICAL BACKGROUND AND METHODOLOGY

3.1. Resolution of the Radiative Transfer Equation (RTE) by the four-flux method

Rayleigh and Mie theories[11,12] account for the light wave propagation through a homogeneous medium that contains spherical scattering (and possibly absorbing) heterogeneities randomly dispersed. In 1960, Chandrasekhar[13] established the radiative transfer equation (abbreviated RTE hereafter) that describes the light interactions of scattering centers with a complex refractive index $N_p(\lambda)$ ($N_p(\lambda) = n_p(\lambda) + i\,k_p(\lambda)$ with p for particle, n_p the real part and k_p the imaginary part) embraced in a medium of thickness dZ with a real refractive index n_m. These scattering particles are characterized by their absorption (K) and scattering (S) coefficients wavelength dependent, such as $K(\lambda) = pC_{abs}(\lambda)$ and $S(\lambda) = pC_{sca}(\lambda)$, with p the number of particles per volume unit ($p = c/V$ with c the volume fraction of particles in the medium, V the volume of a spherical particle) and $C_{abs}(\lambda)$ and $C_{sca}(\lambda)$ the absorption and scattering cross-sections, respectively. Actually, $C_{abs}(\lambda)$ is related to the capacity of an heterogeneity to extract, partially or totally, a wave radiation of the incident visible range (the energy is then released as heat, i.e. infrared radiations in most of the cases) while $C_{sca}(\lambda)$ reflects the ability of a scattered entity to change the direction of the incident light, thus to remove partially or totally a wave radiation of the incident visible range in a given direction. A scattering cross-section should not be interpreted as a true geometric cross-sectional area, but as an effective area that is proportional to the probability of interaction between the radiation and target. Thus, the total attenuation of the incident light will depend on the extinction cross-section C_{ext}, defined as $C_{ext} = C_{abs} + C_{sca}$. C_{ext} and C_{sca} can be expressed as follow:

$$C_{ext} = \frac{2\pi}{k^2}\sum_{n=1}^{\infty}(2n+1)\ Re(a_n + b_n) \text{ and} \quad (1)$$

$$C_{sca} = \frac{2\pi}{k^2}\sum_{n=1}^{\infty}(2n+1)(|a_n|^2 + |b_n|^2) \quad (2)$$

with $k = 2\pi n_m/\lambda_0$ (n_m and λ_0 are the refractive index of the medium, and the incident wavelength in vacuum or air, respectively). a_n and b_n are the Mie scattering coefficients (according to Ricatti-Bessel functions[14]) that depend on the size parameter (i.e. ka where a is the radius of the scattering spheres) and the refractive indices ratio N_p/n_m (N_p is the complex refractive index of the scattering species). Re stands for real part in opposition to imaginary part of the complex optical index.

Several methods have been developed to solve the RTE that allows the modeling of the luminous fluxes balance into a given layer, as shown in the **Figure 2a**. Our study is based on the four-flux model developed by Maheu *et al*[15] that is sketched up in **Figure 2b**. Namely, a collimated incident beam passes through a layer and can be divided in four fluxes: a collimated flux I_c and a semi-isotropic diffuse flux I_d onwards, and a collimated flux J_c and a semi-isotropic diffuse flux J_d backwards. The equations are given by:

$$\frac{dI_c}{dZ} = (K+S)I_c \quad (3)$$

$$\frac{dJ_c}{dZ} = -(K+S)J_c \quad (4)$$

$$\frac{dI_d}{dZ} = \varepsilon(K + (1-\zeta_d)S)I_d - \varepsilon(1-\zeta_d)SJ_d - \zeta_c SI_c - (1-\zeta_c)SJ_c \quad (5)$$

$$\frac{dJ_d}{dZ} = -\varepsilon(K + (1-\zeta_d)S)J_d + \varepsilon(1-\zeta_d)SI_d + \zeta_c SJ_c + (1-\zeta_c)SI_c \qquad (6)$$

ζ_d and ζ_c are the onwards fractions for the diffuse and the collimated beams, respectively whereas $(1-\zeta_d)$ and $(1-\zeta_c)$ are the related backwards fractions. These two coefficients are calculated, like the cross sections, from Mie theory. ε is a multiplication factor fixed between one to two and commonly uses to account for the average path-length of light within a dZ thick slice. For a collimated beam normal to the surface with no scattering, ε equals 1. In contrast, when the scattering is isotropic, or when it is anisotropic but multiple scattering phenomena are at work, ε rather tends towards 2.

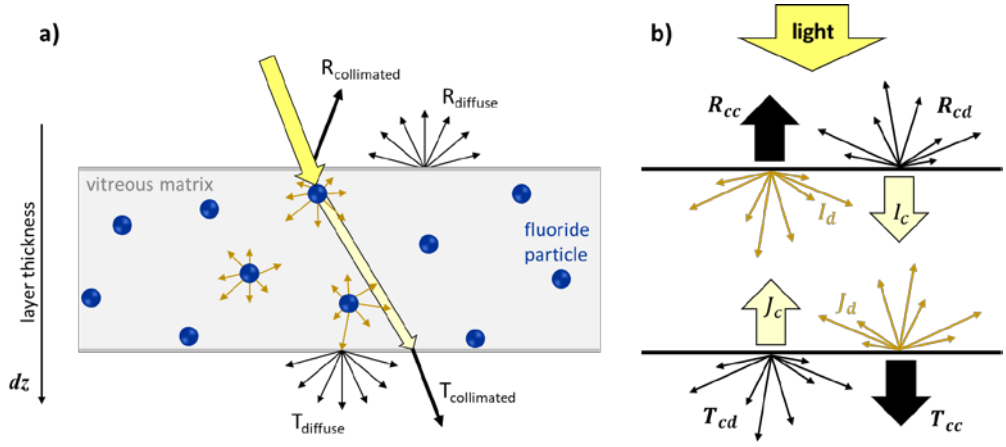

Figure 2 : a) Reflection and transmission effects with the two behaviors, collimated and scattered beams (R stands for reflection, T for transmission). b) Four fluxes propagation (two collimated beams I_c and J_c, and two diffuse beams I_d and J_d) into a slice. The model calculates the four resulting coefficients: R_{cc}, R_{cd}, T_{cc}, and T_{cd}, R_{cc}: Reflection (collimated → collimated), R_{cd}: Reflection (collimated → diffuse), T_{cc}: Transmission (collimated → collimated), T_{cd}: Transmission (collimated → diffuse).

From equations 4 to 7, the intensities of the specular and the scattered reflected beams (hereafter labeled Rcc and Rcd, respectively) and the specular and the scattered transmitted beam (hereafter labeled Tcc and Tcd, respectively) can be calculated (here the cc and cd subscripts stand for collimated → collimated and collimated → diffuse interactions, respectively). The R_{dd} and T_{dd} terms (diffuse→diffuse interactions) are not taken into account hereafter, experimental data being collected with a collimated beam.

3.2. Four-flux model configuration

Throughout the study, the four-flux model is used to simulate the light interaction within matter in the visible spectral range, i.e. from 380 to 780 nm. The following conditions were applied:

- A 3.5 mm thick infinite layer surrounded by air (n=1) on both sides was considered.
- The primary beam is collimated (only one incident direction) and unpolarized with a normal incidence (incidence angle of 0°).
- The refractive index $n_m(\lambda)$ of fused silica was chosen for the medium, SiO_2 being the major constituent of the glassy matrix.
- The refractive index of NaF (as for CaF_2 and SiO_2) was extracted from the Crystran data base[16].
- The average crossing parameter ε is equal to 2 due to several parameters related to the layer (large thickness, relatively high inclusion concentration and size).

R_{cc} and R_{cd} reflectance spectra, and T_{cc} and T_{cd} transmittance ones were calculated for different average and variance particle sizes, and concentrations. R_{cc} spectra (collimated-collimated reflectance) are not depicted hereafter because the $R_{cc}(\lambda)$ values are almost constant whatever the inputs and equal at ca. 4 %. Let us notice here the proper knowledge of the crystallized phases (chemical composition and crystal (particle) size) is of capital importance as inputs to avoid simulations far away from reality.

3.3. CIE L*a*b* colorimetric parameters (and transparency vs. opacity)

Lab colorimetric parameters were calculated in the CIE Lab 1976 color space for a 10° standard observer from simulated reflected light beam with the CIE Standard illuminant D65. Two configurations were envisioned, namely a plate on a black substrate and a plate on a white substrate, to account for the visual rendering (and especially, the transparency) of the prepared colorless glass-ceramics (**Figure 3**). According to the CIE definitions[17], a material will be considered as fully transparent when the transmitted light originates only from the collimated flux (T_{cc}). In contrast, a material will be regarded as translucent when the transmitted light contains a (significant) scattered contribution (T_{cd}). Whatever, transmitted light will be totally absorbed by a black substrate, and totally reflected by a white substrate. Consequently, only the reflection R(λ) will contribute to the determination of Lab parameters in the former case, while the reflection R(λ) and the square of the transmission T(λ) will be taken into account in the latter case (i.e. R(λ) vs. R(λ) + T(λ)^2).

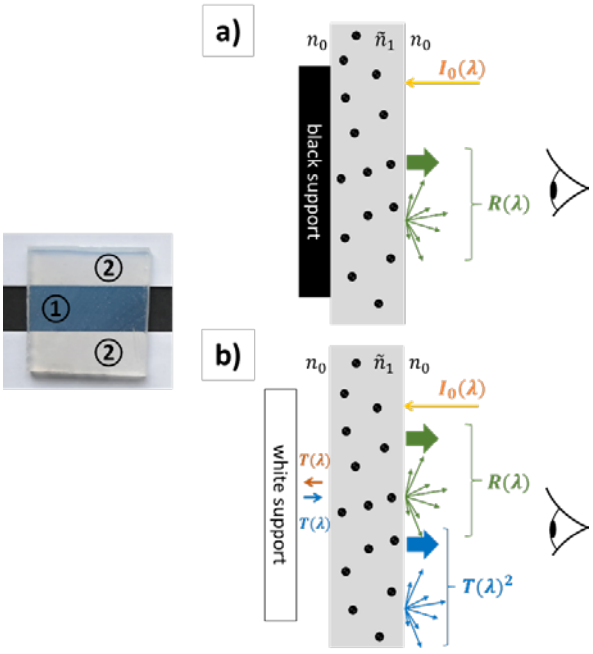

Figure 3: Schematic representations of luminous fluxes consideration into the Lab parameter calculation a) from the total reflectance on a black support and b) from the total reflectance on a white support.

4. REFLECTANCE AND TRANSMITTANCE MODELING

The first aim of the present work was to identify the salient parameters that impact on the color rendering of the studied glass ceramics. In that context, variable parameters that are feature to particles dispersed in the matrix (their size, their size distribution, their volume fraction, their refractive index, etc.) were treated separately.

4.1. Refractive index *n* of the scattering centers

As previously discussed, the prepared opal glasses contain two distinguishable crystalline scattered centers, i.e. NaF and CaF_2. CaF_2 presents a refractive index quite similar to the one of vitreous matrix, while $n(\lambda)_{NaF}$ is significantly lower than $n(\lambda)_{SiO2}$ in the visible range (**Figure 4**). Consequently, as scattering phenomena strongly depend on the N_p/n_m ratio, the impact of NaF on light diffusion is expected to be much more pronounced than the one of CaF_2.

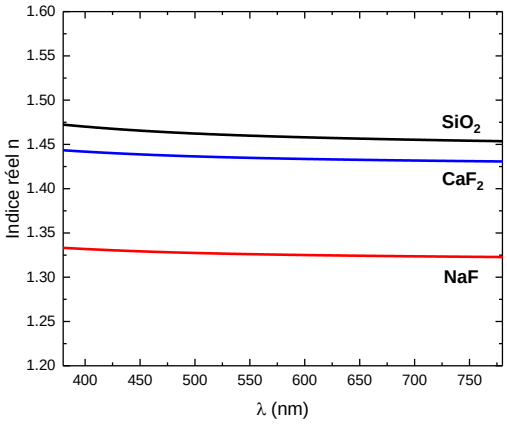

Figure 4: Refractive indexes of the SiO2-based matrix and crystalline phases, NaF and CaF2 in the 380-780 nm wavelength range [16].

This is clearly observed in **Figure 6a** for 100 nm diameter nanoparticles of NaF and CaF_2 dispersed in a SiO_2 vitreous glass with a volume percentage of 5%. Clearly, R_{cd} values are much higher for NaF scattered centers (from ca. 0.9 to 0.5 for λ ranging from 380 nm to 780 nm) than CaF_2 one (from ca. 0.4 to 0.05), while the inverse trend is observed for T_{cd} ones (from ca. 0.0 to 0.1 for NaF and 0.2 to 0.9 for CaF_2). CaF_2 based composite present a typical Rayleigh behavior due to the relatively small size but above all to the small difference in optical indices: the short wavelengths are more scattered (in transmission and reflection) and the longest wavelengths pass through the thickness without being scattered. Compared to NaF, CaF_2 based composites will strongly reflect the blue light and will very slightly transmit the red light. NaF composites present a characteristic Mie behavior, all wavelengths are scattered, with a preference for the shortest, the reflectance is strong for all wavelength, but higher for the shortest wavelength. In our case of a relatively thick sample, the collimated transmission tends to zero, so, according to the energy conservation, the diffuse transmittance is low, but slightly higher for the longest wavelengths. Consequently, the larger the difference of refractive index between the inclusion and the glass, the more the R_{cd}, the more pronounced the opalescent effect, i.e. the more intense the milky feature. Thus, we can conclude that NaF plays the major role in the whitening of our opal glasses and CaF_2 reinforce the whitening phenomenon at the margin in very first sight. To simplify the task, only NaF particles will be considered in the forthcoming simulations.

4.2. Particle size ø

The particle size can change significantly the overall scattering effect within both the Rayleigh and the Mie regimes[18–21]. In our case, the crystallite (particle) size ranges approximately between 20 nm and 200 nm as a function of the concentration in fluoride inserted in the glass

ceramics. Clearly, from the examination of the **Figure 6b** (NaF Vol. of 5%), it appears obvious that the larger the NaF particles, the lower the collimated transmission (T_{cc}) and the higher the diffuse reflection (R_{cd}) with a systematic red shift of the spectra. A ten-fold increase of the particle can have a drastic influence on T_{cc} and R_{cd}. For instance, for 20 nm ø particles, the collimated beam extinction is almost null as T_{cc} tends toward 90 % at high wavelengths. In contrast, T_{cc} tends toward zero as soon as particle diameter exceeds 100 nm. On the contrary and as expected, the larger the NaF particle size, the higher the scattered fluxes (R_{cd} and T_{cd}). The set of curves clearly shows the transition from Rayleigh's regime to that of Mie mentioned above. Between the two, the diffuse transmittance, highest for the short wavelengths in the case of Rayleigh and for the long wavelengths in the case of Mie, can present a maximum which will shift towards the long wavelengths with increasing size.

4.3. Particle size distribution σ

In a glass ceramic, nanocrystals that play the role of scattered centers do not necessary reach the same size at the end of the crystallization process. Consequently, the composite materials should be characterized by a mean value of the particle size and its variance, that is the average of the squared differences from the mean value. Indeed, the influence on the scattering phenomenon of the particle size distribution has to be considered. As sketched up in **Figure 5**, three mean particle diameters have been chosen (50, 100 and 200 nm) for simulations with size distributions (σ) of 10, 20 to 30 %.

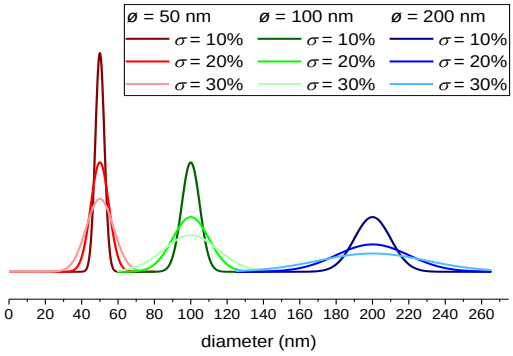

Figure 5: Gaussian functions representing all size distributions modeled for each fixed particle diameter, 50 nm (blue), 100 nm (red) and 200 nm (green).

The results of this parameter variation are reported in **Figure 6c**. As for the observations made for the monodisperse particle size variation, the collimated fluxes decrease when the size distribution gets high. For all simulated cases, T_{cc} is quite negligible, except in the case of a 50 nm diameter particle where it decreases with the size distribution increase. The most important effect of the size distribution can be observed on the coefficient R_{cd}. In fact, the light reflected in all directions represents 90 % of the incoming light in the visible range for a particle of 200 nm with a high size distribution (≥ 30 %). Therefore, above 100 nm as diameter particle, T_{cd} decreases with the size distribution increase. In our case of relatively small sizes, increasing the width of the size distribution is the same as slightly increasing the size.

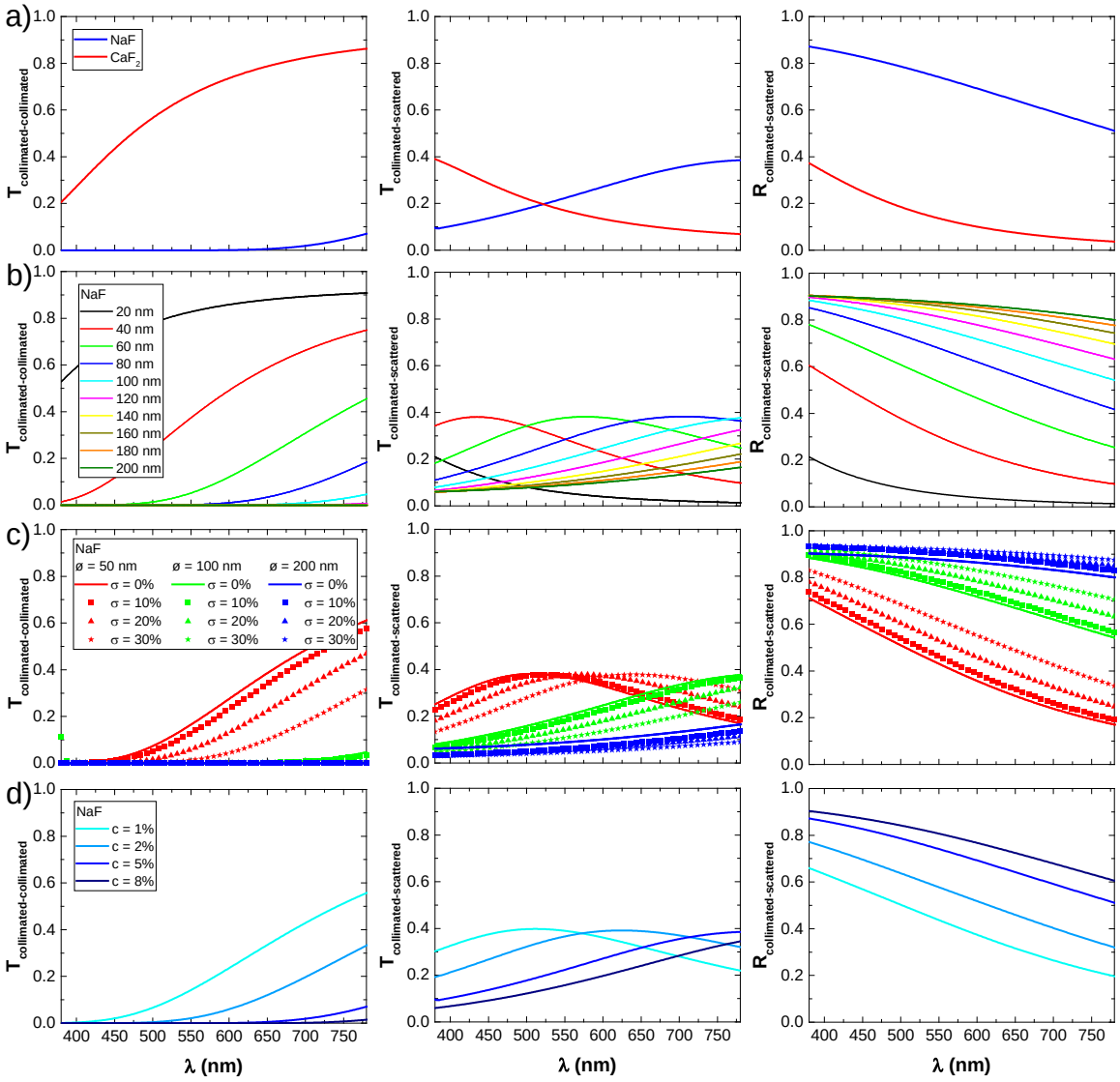

Figure 6: Spectra modeled from intrinsic structural and microstructural parameter values. Left column: collimated-collimated, middle column: collimated-scattered transmittance, right column: collimated-scattered reflectance. a) variation of refractive index by changing the particle nature, NaF and CaF_2, (others parameters : ø = 100 nm, σ = 0), b) effect of NaF particle size in the 20-200 nm diameter range (others parameters : c = 4.7 %, σ = 0), c) variation of polydispersity for 50, 100 and 200 nm in diameter NaF particles (other parameter : c = 4.7 %), d) variation of NaF particle volume fraction from 1 to 8 % (others parameters : ø = 100 nm, σ = 0).

4.4. Particle volume fraction *c*

The particle volume fraction must be very low to fulfill the Radiative Transfer Equation (RTE), in order to minimize and disregard the potential interactions between particles. Namely, high inter-particle distances with an order of magnitude much greater than the wavelength are necessary. As shown in **Figure 6d**, the concentration values ranging from 1 % to 8 % could be considered as too high to satisfy the RTE model. However, the particle size being very small, around 100 nm in diameter, makes it possible to consider that the inter-particle distance remains greater than the wavelength.

The coefficient T_{cc} decreases significantly as the particle concentration in the matrix increases. Besides, no collimated transmission is assumed anymore above a 5 % volume concentration. On the contrary, the higher the particle volume fraction, the higher the coefficient R_{cd}. It reaches 80 % for a 8 % NaF volume fraction. Then, the coefficient T_{cd} passes through a maximum of 40 % for volume fractions from 1 to 5 %. Beyond this last value, T_{cd} is lower in the visible wavelength range.

5. EXPERIMENTAL VALIDATION OF THE MODEL

In order to validate the model, calculations of transmission and reflection spectra have been realized by the four-flux model from NaF crystals parameters obtained through XRD analysis (Table 1). Then, a comparison between Lab parameters from measurements (Table 2) and simulations has been done (Table 3). Measured Lab coefficients were determined thanks to the use of a Perkin Lambda 1050 as well as a DatacolorCheck III spectrophotometer.

Table 2: Lab parameters, considering white and black substrates, calculated from experimental reflection spectra (obtained by integrating sphere).

	white substrate			*black substrate*		
%wt of fluorine	**L**	**a**	**b**	**L**	**a**	**b**
2.9	96.23	-0.08	2.33	38.86	0.84	-11.55
3.6	93.07	-0.84	-4.01	90.91	-2.21	-6.46
3.8	94.66	-0.92	-3.10	93.57	-1.63	-4.28
4.1	96.88	-0.47	-1.25	96.57	-0.60	-1.49

Table 3: Lab parameters, considering white and black substrates, calculated from modeled reflection spectra (obtained by four flux method).

	white substrate			*black substrate*		
%wt of fluorine	**L**	**a**	**b**	**L**	**a**	**b**
2.9	95.73	-0.06	2.80	41.45	0.91	-13.12
3.6	93.26	-1.09	-3.78	91.23	-2.59	-6.03
3.8	94.81	-1.07	-2.77	93.79	-1.79	-3.81
4.1	96.86	-0.54	-1.21	96.55	-0.68	-1.45

When the concentration of fluorine increases, the size of the scattering particles is enhanced. Consequently, this triggers naturally a change in the light scattering regime from the Rayleigh model to the Mie one with a tint shifting concomitantly from blue to white. For glass-ceramic samples on a black substrate, luminance shifts from low to high with fluorine amount in relation with a rise of the scattering phenomenon (no light can be reflected by the substrate). The overall feature of the samples changes from bluish ($a \approx 0$, $b < 0$, L low) to bright white ($a \approx 0$, $b \approx 0$, L high). In contrast, for glass-ceramic samples on a white substrate, the L value first decreases for fluorine percentage going from 2.9 to 3.6, and then increases for larger concentration (from 3.6 to 4.1 wt%). Namely, if the glass-ceramic is transparent (e.g. 2.9%wt of fluorine), the white substrate contributes significantly by reflecting the impinging white light. This results in a high L parameter. When the glass-ceramic becomes more translucent or opaque, i.e. when the light

is (strongly) scattered, the white substrate contributes less. Then, the L parameter gets higher only because of the higher concentration and particle size of NaF (e.g. 3.6 to 4.1%wt of fluorine).

In order to evaluate the color difference between the two Lab parameter sets, the CIEDE2000 formula has been used[22] (only on white support). The calculation results, ΔE_{00}, are reported in Table 4. According to the literature[23], a standard observer is not able to notice a difference between two samples with a ΔE value of 0 to 1. All obtained ΔE_{00} (**Table 4**) are less than 1. This allows to validate the modeling of reflection and transmission spectra by the four-flux model for studied opal glasses.

Table 4: Color difference ΔE_{00} calculated between Lab parameters from experimental reflection spectra and modeled reflection spectra (considering white substrate).

%wt of fluorine	ΔE_{00}
2.9	0.52
3.6	0.43
3.8	0.38
4.1	0.11

Based on the calculated Lab coefficients, a simulation of the optical rendering of the studied samples on black and white supports was achieved and compared to reality **(Figure 7).** The appearance modeling from both ways, measurement with a spectrophotometer and calculations by the four-flux model, are really similar. It provides that in our case the four-flux model gives a correct appraisal of reflection and transmission fluxes when material intrinsic physical parameters are known.

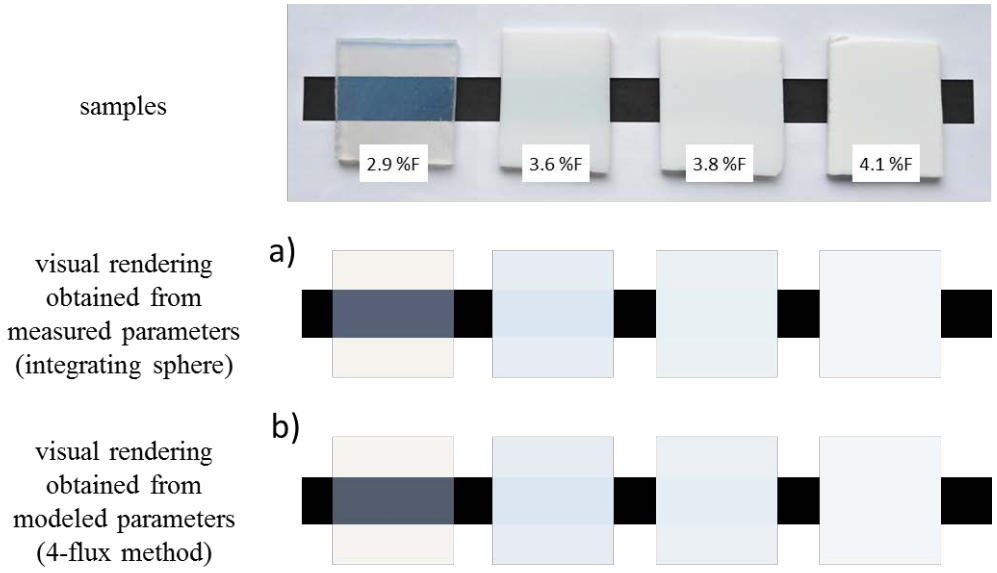

Figure 7: Comparison of transparency modeling from collimated transmission determined by integrating sphere (b), and calculated by the four-flux model (c)

6. CONCLUSION AND PERSPECTIVE

As it has been exposed in this article, the RTE solving through the four-flux model allows to determine reflection and transmission spectra from a scattered layer whose inclusions are small

and in a low enough concentration. From these simulations, a reliable rendering of the material can be obtained in terms of both colorimetric and transparency aspects. Thereby, the four-flux method is well adapted to predict the visual appearance of a partially crystallized glass like the opal glass.

The aim of this work was to establish the microstructural parameter influences on the scattering effect in an opal glass. The main important parameter concerns inclusions refractive index that has to be as different as possible from that of the matrix. First, the inclusions refractive index needs to be really different of the matrix one as the NaF particles, here. Then, the increasing of all others parameters intensifies the scattering effect.

In the near future, the modeling through the RTE solving by the four-flux model will be extend to opal glasses colored by mineral pigments. In this case, the challenge will be to simulate the balance between both scattering and absorption phenomena.

REFERENCES

(1) Houdaer, J.-P. La Coloration Des Verres. *Verre* **2005**, *11* (4), 4–16.

(2) Lafait, J.; Berthier, S.; Andraud, C.; Reillon, V.; Boulenguez, J. Physical Colors in Cultural Heritage: Surface Plasmons in Glass. *Comptes Rendus Phys.* **2009**, *10* (7), 649–659.

(3) Welter, N.; Schüssler, U.; Kiefer, W. Characterisation of Inorganic Pigments in Ancient Glass Beads by Means of Raman Microspectroscopy, Microprobe Analysis and X-Ray Diffractometry. *J. Raman Spectrosc.* **2007**, *38* (1), 113–121.

(4) Pouyet, E.; Cotte, M.; Fayard, B.; Salomé, M.; Meirer, F.; Mehta, A.; Uffelman, E. S.; Hull, A.; Vanmeert, F.; Kieffer, J.; Burghammer, M.; Janssens, K.; Sette, F.; Mass, J. 2D X-Ray and FTIR Micro-Analysis of the Degradation of Cadmium Yellow Pigment in Paintings of Henri Matisse. *Appl. Phys. A* **2015**, *121* (3), 967–980.

(5) Elias, M.; Lafait, J. *La Couleur. Lumière, Vision et Matériaux: Lumière, Vision et Matériaux*; Humensis, 2015.

(6) Neuville, D. R.; Cormier, L.; Caurant, D. *Du verre au cristal: Nucléation, croissance et démixtion, de la recherche aux applications*; EDP Sciences, 2013.

(7) Deubener, J.; Allix, M.; Davis, M. J.; Duran, A.; Höche, T.; Honma, T.; Komatsu, T.; Krüger, S.; Mitra, I.; Müller, R.; Nakane, S.; Pascual, M. J.; Schmelzer, J. W. P.; Zanotto, E. D.; Zhou, S. Updated Definition of Glass-Ceramics. *J. Non-Cryst. Solids* **2018**.

(8) Zanotto, E. D. Bright Future for Glass-Ceramics. *Am. Ceram. Soc. Bull.* **2010**, *89* (8), 19–27.

(9) Lord Rayleigh. On the Transmission of Light through an Atmosphere Containing Small Particles in Suspension, and on the Origin of the Blue of the Sky. *Lond. Edinb. Dublin Philos. Mag. J. Sci.* **1899**, *47* (287), 375–384.

(10) Bohren, C. F.; Huffman, D. R. *Absorption of Light by Small Particles*; Wiley; 1983.

(11) Mie, G. Beiträge Zur Optik Trüber Medien, Speziell Kolloidaler Metallösungen. *Ann. Phys.* **1908**, *330* (3), 377–445.

(12) Strutt, H. J. W. On the Light from the Sky, Its Polarization and Colour. *Lond. Edinb. Dublin Philos. Mag. J. Sci.* **1871**, *41* (271), 107–120.

(13) Chandrasekhar, S. *Radiative Transfer*, Dover.; 1960.

(14) Wiscombe, W. J. Improved Mie Scattering Algorithms. *Appl. Opt.* **1980**, *19* (9), 1505–1509.

(15) Maheu, B.; Letoulouzan, J.-N.; Gouesbet, G. Four-Flux Models to Solve the Scattering Transfer Equation in Terms of Lorenz-Mie Parameters. *Appl. Opt.* **1984**, *23* (19), 3353–3362.

(16) Crystran. Https://Www.Crystran.Co.Uk/Optical-Materials.

(17) CIE. *International Lighting Vocabulary*; 17.4; CIE Publication: Vienna: Central Bureau of the CIE, 1987.

(18) Shioya, K.; Komatsu, T.; Kim, H. G.; Sato, R.; Matusita, K. Optical Properties of Transparent Glass-Ceramics in K2O-Nb2O5-TeO2 Glasses. *J. Non-Cryst. Solids* **1995**, *189* (1–2), 16–24.

(19) Shahmiri, R.; Standard, O. C.; Hart, J. N.; Sorrell, C. C. Optical Properties of Zirconia Ceramics for Esthetic Dental Restorations: A Systematic Review. *J. Prosthet. Dent.* **2018**, *119* (1), 36–46.

(20) Wang, F.; Gao, J.; Wang, H.; Chen, J. Flexural Strength and Translucent Characteristics of Lithium Disilicate Glass–Ceramics with Different P2O5 Content. *Mater. Des.* **2010**, *31* (7), 3270–3274.

(21) Beall, G. H.; Pinckney, L. R. Nanophase Glass-Ceramics. *J. Am. Ceram. Soc.* **1999**, *82* (1), 5–16.

(22) Commission Internationale de l'Eclairage. *Colorimetry: Technical Report*; Central Bureau of the CIE, 2004.

(23) Mokrzycki, W. S.; Tatol, M. Colour Difference Delta E - A Survey. *Mach. Graph. Vis.* **2011**, *20* (4), 383–412.